PAPER

Check for updates

Acid vapor doping of polar polythiophenes for high electrical conductivity†

Yu Qiu,[ab] Fei Zhong,[ac] Zhen Xu,[ac] Jian Song,[d] Ke Shen,*[b] Hui Li*[ac] and Lidong Chen [ID] *[ac]

An ideal doping process should be highly efficient and avoid the disruption of molecular packing to achieve the synergistic optimization of carrier concentration and mobility. Herein, we synthesized two polythiophene derivatives with oligo ethylene glycol as side chains and thienothiophene (bithiophene) as unit, denoted Pg_32T-TT (Pg_32T-2T). A strong acid, trifluoromethanesulfonic acid (TfOH), was used as dopant to elucidate the effects of two doping methods, solution- and vapor-doping without ultrahigh vacuum, on the polar polythiophenes' electrical properties. Notably, the σ of vapor-doped films were two times higher than those of solution-doped counterparts. Specifically, TfOH vapor-doped Pg_32T-TT achieved a remarkable σ value of up to 1173.9 S cm^{-1}, among the highest values of polar polythiophenes. The high σ of vapor-doped films was attributed to the increased carrier concentrations without degradation of mobilities, which indicates that vapor doping enables more effective doping reactions with maintained crystallinity, compared with solution doping, because acid vapor molecules directly diffuse into the polar side chains of pure polymers as confirmed by grazing-incidence wide-angle X-ray scattering. Moreover, TfOH-doped films exhibited exceptional air stability stored in air for over one month. This work demonstrates that TfOH vapor doping without ultrahigh vacuum conditions represents a promising approach for improving the electrical conductivity and stability of conductive polymers for flexible electronics.

1 Introduction

Conjugated polymers have attracted great interest in application of organic electronics, attributed to their solution processessability, low toxicity, intrinsically light weight and mechanical flexibility.[1–3] Achieving high electrical conductivity (σ) in conjugated polymers is crucial to fulfill their diverse applications in flexible electronic devices.[4,5] Chemical doping can efficiently boost the number of charge carriers in polymer films, facilitating trap filling and subsequently enhancing electrical conductivity ($\sigma = ne\mu$, n is carrier concentration, μ is mobility and e is elementary charge).[6–8] The critical challenge lies in elevating n while maintaining a sufficiently high μ because the

[a]State Key Laboratory of High Performance Ceramics and Superfine Microstructure, Shanghai Institute of Ceramics, Chinese Academy of Sciences, Shanghai 200050, China. E-mail: lihui889@mail.sic.ac.cn; cld@mail.sic.ac.cn

[b]College of Materials Science and Engineering, Hunan University, Changsha 410082, China. E-mail: shenk@hnu.edu.cn

[c]Center of Materials Science and Optoelectronics Engineering, University of Chinese Academy of Sciences, Beijing 100049, China

[d]School of Microelectronics, Shanghai University, Shanghai 201800, China

† Electronic supplementary information (ESI) available: Additional details include synthetic procedures, characterization data, descriptions of experimental methods, additional figures and tables of GPC, TGA, DSC, CV, GIWAXS, AFM, electrical conductivity data. See DOI: https://doi.org/10.1039/d5ra03453a

addition of a large amount of dopants leads to the disruption of polymer packing and thus hinder the charge transport.[9] Rational molecular design, including polymer backbone[10–12] and side chain engineering,[13–15] as well as the proper choice of dopants,[16–18] have been proved to optimize the carrier concentration with improved molecular packing, and thus effectively enhance polymers' electrical conductivities.

Several doping approaches have been developed to avoid detrimental impacts on the microstructure during the doping process.[19,20] A good example is sequential processing, involving stepwise deposition of a polymer semiconductor and a dopant.[21–23] Evaporating the dopant molecule on top of a polymer film pre-deposited by spin coating[24–26] (vapor doping) also allows minimal morphological damage to the film and maintains efficient transport paths. By using vapor doping, Sirringhaus et al. reported a highly ordered PBTTT film by diffusing dopants into electrically insulating side chain, resulting in a high conductivity up to 1000 S cm^{-1} even at high doping levels.[27] The choice of dopants for vapor doping is crucial for the doping efficiency and stability of doped films. CF_3SO_3H (TfOH) with its ability to protonate electron-rich organic semiconductors, has been demonstrated to enhance the σ of conductive polymers by solution doping.[28,29] Very recently, typical polymer PEDOT:PSS treated with TfOH vapor, exhibited high σ of 2053 S cm^{-1} and exceptional thermal

stability,[30] demonstrating the ability of TfOH for efficient doping. Thiophene polymers with polar side chains are promising conductive polymers for flexible electronics.[31,32] However, their doping with strong acids has been rarely explored, primarily due to concerns regarding their instability in ambient conditions. It is intriguing to explore how TfOH vapor doping influences the electrical properties of these polar polythiophenes.

Herein, two oligo ethylene glycol substituted polythiophenes, Pg$_3$2T-TT and Pg$_3$2T-2T, were synthesized. A strong acid, TfOH, was used as dopant by vapor doping and solution doping to improve the electrical properties of these polymers (Fig. 1). It is found that the vapor-doped Pg$_3$2T-TT and Pg$_3$2T-2T exhibit high σ among the highest values of polar polythiophenes. It is proved that higher doping efficiency by vapor doping compared with solution doping is responsible for the high σ while the strong interaction of vapor dopants with side chains is beneficial for carrier delocalization along backbone and contributes to the stability of doped films. Our results demonstrate that TfOH vapor doping without ultrahigh vacuum condition is an effective approach to enhance electrical conductivity and stability of conductive polymers.

2 Results and discussion

2.1 Synthesis and characterization of polymers

Pg$_3$2T-TT and Pg$_3$2T-2T were synthesized using Stille coupling (Scheme S1†) and the synthetic details are shown in the experimental section. Both polymers have high molecular weights (ESI Fig. S1 and Table S1†) and good thermal stability with a decomposition temperature around 250 °C (ESI Fig. S2†). No distinctive transition peak observed at temperature range of 25–250 °C (ESI Fig. S3†). The polymers were doped by two methods, solution doping and vapor doping, as illustrated in ESI Fig. S4.† For solution doping processing, the polymer solution and dopant

solution are mixed with the desired concentration, then the single solution is drop-casted on the substrate to form doped films. For vapor doping processing, the thin films are prepared by drop-casting, and then the as-cast neat films are placed into a glass lid filled with dopant vapor for a suitable doping time to get the vapor-doped films. The doping level of polymer films is modulated by the molar ratio (MR) of TfOH to polythiophene (repeating unit) and the vapor exposure time, respectively.

Cyclic voltammetry (CV) measurements show that the highest occupied molecular orbital (HOMO) levels of Pg$_3$2T-TT and Pg$_3$2T-2T are −4.74 eV and −4.55 eV, respectively (ESI Fig. S5†). Density functional theory (DFT) calculations also showed that the repeat unit of Pg$_3$2T-2T has a higher-lying HOMO level compared with the repeat unit of Pg$_3$2T-TT, indicating Pg$_3$2T-2T
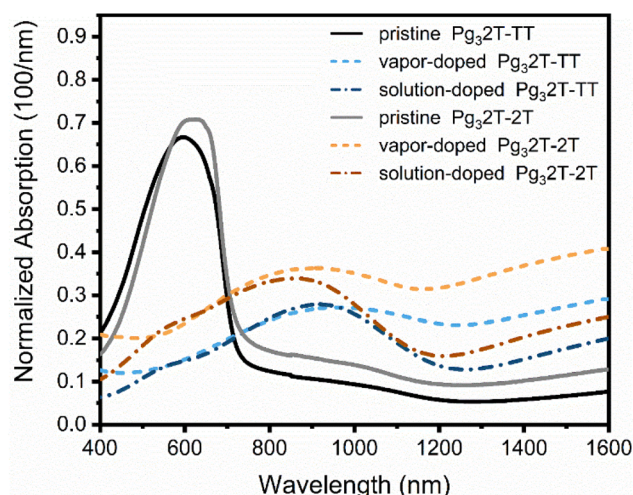

Fig. 2 The thickness-normalized UV-vis-NIR absorption spectra of pristine and doped films (vapor doping time is 2 min and the MR for solution doping is 0.6).
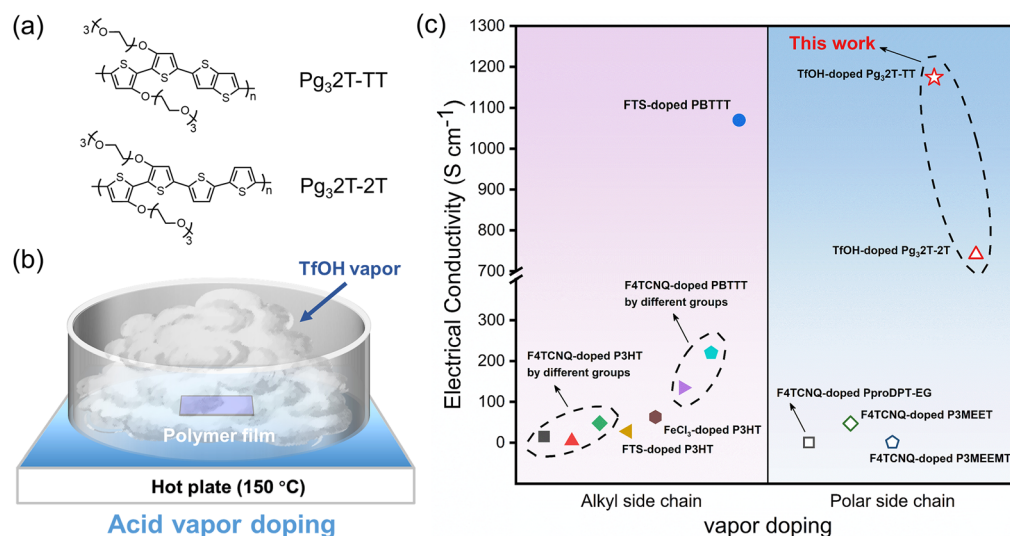

Fig. 1 (a) Chemical structure of Pg$_3$2T-TT and Pg$_3$2T-2T. (b) Schematic illustration of doped films prepared by acid vapor doping method. (c) Electrical conductivities for typical vapor-doped polythiophenes with/without polar side chains (detailed data are listed in Table S2†).

more easily doped by dopants (ESI Table S3†). Both of two polymers are prone to be oxidized in air due to their high-lying HOMO energy levels, supported by the UV-vis-NIR absorption spectra (Fig. 2). It is observed that these polymers can be effectively doped by TfOH both by vapor and solution methods. The neutral absorption bands at 400–650 nm for Pg$_3$2T-TT and Pg$_3$2T-2T were significantly bleached with a pronounced enhancement of absorption intensity at near-infrared (NIR) band (800–1600 nm). Pg$_3$2T-2T films exhibited stronger (bi) polaron peaks upon doping, consistent with its higher-lying HOMO level. It is observed that vapor doping resulted in a stronger NIR absorption band compared to solution doping, indicating a higher doping level obtained by vapor doping.

Raman spectra were performed to further detect the doping level of different doping methods (Fig. 3). The peak of Pg$_3$2T-TT at 1408 cm^{-1} corresponds to C=C stretching on the thienothiophene ring, while the peaks at 1447 cm^{-1} and 1496 cm^{-1} are attributed to C=C stretching and C=C/C–C stretching/shrinking on the thiophene ring, respectively. Upon doping, the peak intensities at 1408 cm^{-1} and 1496 cm^{-1} are significantly attenuated, and the peak at 1447 cm^{-1} red-shifted to 1434 cm^{-1}. Concurrently, the peak intensity at 1310 cm^{-1}, corresponding to C=C/C–C stretching/shrinking on the thienothiophene ring, increases remarkably, indicating the doping reaction mainly occurring on the thienothiophene ring. Notably, the attenuation of the peaks at 1447 cm^{-1} and 1496 cm^{-1} is more pronounced in the vapor doping process compared to solution doping, suggesting a higher doping level achieved through vapor doping. For Pg$_3$2T-2T films, the peak at 1447 cm^{-1}, associated with C=C stretching on the thiophene ring, weakens upon doping, while the peak at 1408 cm^{-1}, corresponding to C–C stretching vibrations on the thiophene ring, is slightly red-shifted to 1403 cm^{-1}. Like Pg$_3$2T-TT film, a higher doping level is observed in vapor-doped Pg$_3$2T-2T film, further demonstrating the superior doping efficiency of vapor doping compared to solution doping.

2.2 Electrical property of doped films

The electrical conductivity (σ) of vapor doped films is remarkably higher than those of solution-doped films (Fig. 4). For the vapor doping method, the σ of Pg$_3$2T-TT and Pg$_3$2T-2T achieved the maximum values of 1173.9 S cm^{-1} and 741.2 S cm^{-1}, respectively, when exposed in vapor atmosphere for 2 minutes. For the solution doping method, the maximum σ values of Pg$_3$2T-TT and Pg$_3$2T-2T reach 323 S cm^{-1} and 278 S cm^{-1}, respectively, at a molar ratio of 0.6. These doped films exhibited exceptional air stability since vapor-doped Pg$_3$2T-TT and Pg$_3$2T-2T displayed conductivity losses of ~24% and 27%, respectively, after stored in ambient air for 90 days and the conductivity of solution-doped films mostly unchanged (ESI Fig. S6†). The stability of these films is better than those polythiophenes doped by FeCl$_3$,[29,33] which is probably attributed to the chemical stability of CF$_3$SO$_3^-$ anion and the strong interaction between anions and polar side chains.

Hall effect measurement demonstrates that the high σ of vapor doped films mainly stems from the high carrier
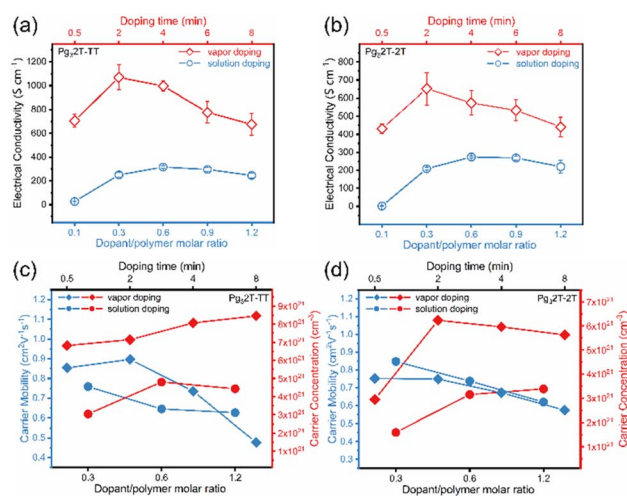
Fig. 4 Electrical conductivity as a function of vapor doping time or molar ratio of dopant to polymer (repeat unit) (a) doped Pg$_3$2T-TT films and (b) doped Pg$_3$2T-2T films. Carrier mobility and carrier concentration as a function of vapor doping time or molar ratio of dopant to polymer (repeat unit) (c) doped Pg$_3$2T-TT films and (d) doped Pg$_3$2T-2T films.
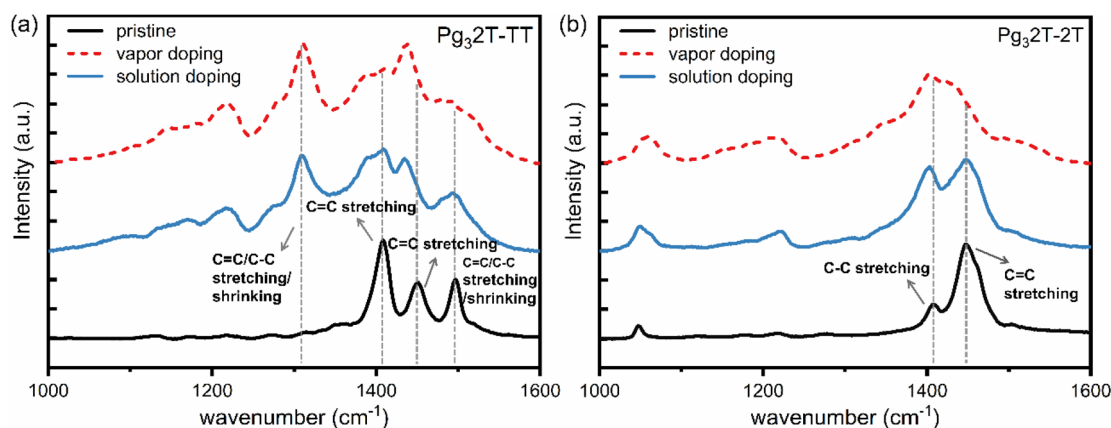
Fig. 3 Raman spectra for pristine and doped films of (a) Pg$_3$2T-TT (b) Pg$_3$2T-2T (the vapor doping time is 2 min and the MR for solution doping is 0.6).

concentrations. In addition, the carrier concentrations of doped $Pg_3$2T-TT films are higher than those of doped $Pg_3$2T-2T film for two methods despite the higher doping levels appearing in latter films in absorption spectra. It implies more (bi)polarons are prone to be free carriers in doped $Pg_3$2T-TT films. The mobilities of vapor doped $Pg_3$2T-TT are slightly higher than those of solution doped films while the mobilities of doped $Pg_3$2T-2T by two methods are almost same. That means the direct diffusion of acid vapor molecules into the pure polymers endows more effective doping reaction compared with the solution doping process in which the existence of solvent may impact the doping level. Temperature-dependent σ measurements show that σ increases with increased temperature, indicating a thermally activated charge transport in these films[11](ESI Fig. S7†). The transport activation energy (E_a) is lower for vapor-doped films compared to those of solution-doped films. Moreover, $Pg_3$2T-TT films have lower E_a values than those of $Pg_3$2T-2T films, indicating lower barriers for (bi)polarons converting to be free carriers in $Pg_3$2T-TT films. This supports the results of higher carrier concentrations in $Pg_3$2T-TT films measured by Hall-effect experiments.

2.3 Microstructure and morphology upon doping

Grazing-incidence wide-angle X-ray scattering (GIWAXS) was employed to analyze the crystalline evolution of pristine films and doped counterparts (Fig. 5a–f). Both pristine $Pg_3$2T-TT and $Pg_3$2T-2T exhibited similar scattering patterns with only edge-

on orientation in films. Upon TfOH doping, the GIWAXS patterns showed more diffraction spots along q_z directions and clearer spots along q_{xy} directions, indicating enhanced crystallinity after doping (peak parameters in ESI Table S4†). For both of two doping methods, the lamellar packing distances of two polymers are increased significantly, while π–π stacking distances are decreased. Although the dopants are prone to inserting into the side chains, vapor-doped films displayed smaller lamellar structure expansion than those of solution-doped films, suggesting limited dopant-induced lamellar distortion during vapor doping. The reduced π–π spacing is attributed to doping-induced polaron delocalization generating strong interchain interaction.[34] Notably, vapor-doped films exhibited narrower diffraction peaks in both out-of-plane (100) and in-plane (010) directions (ESI Fig. S8†). Crystal coherence lengths (CCL) were calculated via Scherrer equation. The vapor-doped films show larger CCLs along both q_z and q_{xy} directions, indicating extended ordered polymer domains, compared with solution-doped films (ESI Fig. S9†). This suggests that the direct diffusion of vapor molecules into the polar side chains of pure polymers improves the film's crystallinity while the microstructure of solution-doped polymer is probably impacted by the evaporation of solvent to form discontinuous transport paths during the film formation. Atomic force microscopy (AFM) revealed the surface roughness is reduced in vapor-doped films while the roughness is significantly increased in solution-doped counterparts compared with pristine films (ESI Fig. S10†). These findings collectively demonstrate that vapor doping minimizes microstructural and morphological disruption. Therefore, the enhanced conductivity by vapor doping in these polymers can be primarily attributed to the synergistic advantages of high doping efficiency of strong acid and the ordered microstructure within continuous conduction pathways inside for efficient charge transport (Fig. 5g).

3 Conclusions

Polythiophene derivatives with polar side chains were synthesized and doped by using a strong acid, CF_3SO_3H (TfOH), via vapor doping and solution doping methods. Both polymers exhibited effective doping reactions while vapor doping leads to higher doping levels compared with the solution doping method. Notably, the σ of vapor-doped $Pg_3$2T-TT film is two times higher than that of solution-doped counterparts. The high σ of vapor-doped films primarily stems from increased carrier concentrations while maintaining ordered domains upon doping. The results indicate that vapor doping is a better choice for achieving high conductivity for polar polythiophenes because the direct diffusion of acid vapor molecules into the polar side chains of pure polymers endows more effective doping reaction, compared with the solution doping process in which the existence of solvent may negatively impact the doping efficiency and morphology. The conductivity of TfOH-doped $Pg_3$2T-TT is reserved over 70% of their initial values even after being stored in air for 90 days. This work demonstrates that acid vapor doping, even without ultrahigh vacuum conditions, is an
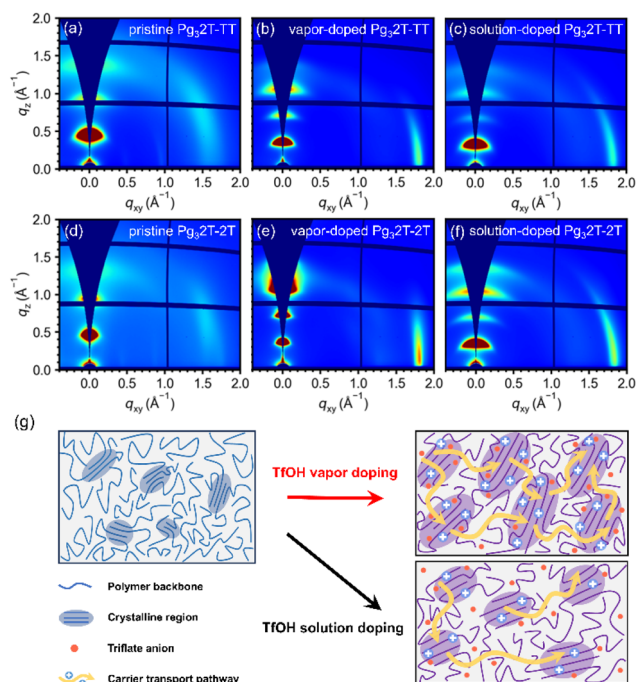
Fig. 5 2D-GIWAXS patterns of (a) pristine $Pg_3$2T-TT (b) vapor-doped $Pg_3$2T-TT (c) solution-doped $Pg_3$2T-TT and (d) pristine $Pg_3$2T-2T (e) vapor-doped $Pg_3$2T-2T (f) solution-doped $Pg_3$2T-2T. (g) Schematic illustration of microstructure in pristine film and doped films by two methods (the vapor doping time is 2 min and the MR for solution doping is 0.6).

efficient approach to enhance both the conductivity and stability of conductive polymers.

4 Experimental

4.1 Films preparation and electrical resistivity measurement

The glass substrate is cleaned by deionized water, acetone and *i*-propanol. The polymers are dissolved in a mixed solvent consisting of chloroform and chlorobenzene (9 : 1, v/v) with the concentration of 5 mg mL^{-1}. For the pristine films, the polymer solutions were stirred at 50 °C for 3 h. Then, the solutions were dropped on the cleaned glass substrates carefully to form thin films. For solution-doped film, 0.02 mol L^{-1} CF$_3$SO$_3$H in acetonitrile was mixed with polymer solutions at the desired concentrations. The mixtures were stirred at 50 °C for 3 h. The single solution then was dropped cast on the substrate. For vapor-doped films, CF$_3$SO$_3$H is dissolved in acetonitrile with the concentration of 1 mol L^{-1}, 200 μL of the dopant solution was dropped on a glass substrate and heated to 150 °C. Polymer films were put in the glass lid with saturated dopant vapor. A four-probe method was used to determine the electrical resistivity and the Seebeck coefficient by using the ZEM-5 TF Seebeck Coefficient/Electrical Resistance Measurement System (Advance Riko). At least three samples were used to measure the resistance and Seebeck coefficient and the average values were reported.

4.2 Hall-effect measurement

For Hall-effect measurement, the device was prepared as the same as for electrical conductivity measurement, and finally four 50 nm Au electrodes were deposited on film to reduce contact resistance.

4.3 DFT simulations

All species were optimized by Gaussian 09 software using the B3LYP functional in the density functional theory (DFT) framework. Furthermore, the Grimme dispersion of the molecular structure with the original D3 damping function was calculated using the 6-31G* basis set.

4.4 Synthesis of polymers

5,5′-Dibromo-3,3′-bis(2-(2-(2-methoxyethoxy)ethoxy)ethoxy)-2,2′-bithiophene (200 mg, 0.31 mmol) and 2,5-bis(trimethylstannyl)thieno[3,2-*b*]thiophene (143.48 mg, 0.31 mmol) were added into a dry Schlenk tube and subsequently dissolved in degassed chlorobenzene (5 mL) under nitrogen atmosphere. The solution was degassed three times. Pd$_2$(dba)$_3$ (5.6 mg, 0.006 mmol) and P (*o*-tol)$_3$ (15 mg, 0.05 mmol) were quickly added and the solution was stirred and degassed for 8 min. The reaction mixture was stirred at 110 °C for 10 min. When the reaction mixture turned to be extremely viscous, it was cooled to room temperature. The mixture was dropped into 200 mL methanol and filtered. The precipitate was collected and purified by Soxhlet extraction with methanol, ethyl acetate and hexane to remove oligomers and impurities. The remaining polymer was dissolved in chloroform and precipitated again into methanol.

The precipitate was collected and dried under vacuum, then the dark polymer was obtained as the product polymer, Pg$_3$2T-TT (117 mg, 60%). M$_n$:73.3 kDa, PDI:4.1.

5,5′-Dibromo-3,3′-bis(2-(2-(2-methoxyethoxy)ethoxy)ethoxy)-2,2′-bithiophene(200 mg, 0.31 mmol) and 5,5′-bis(trimethylstannyl)-2,2′-bithiophene (152.48 mg, 0.31 mmol) were added into a Schlenk tube and subsequently dissolved in degassed chlorobenzene (5 mL) under nitrogen atmosphere. The solution was degassed three times. And then Pd$_2$(dba)$_3$ (5.6 mg, 0.006 mmol) and P(*o*-tol)$_3$ (15 mg, 0.05 mmol) were added and then the solution was stirred and degassed for 8 min. The reaction mixture was stirred at 120 °C for 24 hours. After being cooled to room temperature, the mixture was precipitated in methanol (200 mL) and subjected to a series of Soxhlet extractions successively in hot methanol ethyl acetate and hexane to remove oligomers and impurities, followed by collection in chloroform and precipitation in methanol again. The polymer, Pg$_3$2T-2T, was obtained as dark-blue or metallic solids (145 mg 71%). M$_n$: 28.7 kDa, PDI:8.9.

Data availability

The data supporting this article have been included as part of the ESI.†

Author contributions

The manuscript was written through contributions of all authors. All authors have given approval to the final version of the manuscript.

Conflicts of interest

The authors declare no competing financial interests that might influence this work.

Acknowledgements

References

1 B. Russ, A. Glaudell, J. J. Urban, M. L. Chabinyc and R. A. Segalman, *Nat. Rev. Mater.*, 2016, **1**, 14.
2 H. Ma, H. L. Yip, F. Huang and A. K. Y. Jen, *Adv. Funct. Mater.*, 2010, **20**, 1371–1388.
3 H. Sirringhaus, *Adv. Mater.*, 2014, **26**, 1319–1335.
4 Z. S. Parr, J. Borges-González, R. B. Rashid, K. J. Thorley, D. Meli, B. D. Paulsen, J. Strzalka, J. Rivnay, C. B. Nielsen and J. Borges-González, *Adv. Mater.*, 2022, **34**, 13.

5 N. Kim, S. Lienemann, I. Petsagkourakis, D. A. Mengistie, S. Kee, T. Ederth, V. Gueskine, P. Leclère, R. Lazzaroni, X. Crispin and K. Tybrandt, *Nat. Commun.*, 2020, **11**, 10.

6 B. Lüssem, M. Riede and K. Leo, *Phys. Status Solidi A-Appl. Mat.*, 2013, **210**, 9–43.

7 I. Salzmann, G. Heimel, M. Oehzelt, S. Winkler and N. Koch, *Accounts Chem. Res.*, 2016, **49**, 370–378.

8 B. Lüssem, C. M. Keum, D. Kasemann, B. Naab, Z. N. Bao and K. Leo, *Chem. Rev.*, 2016, **116**, 13714–13751.

9 A. Salleo, R. J. Kline, D. M. DeLongchamp and M. L. Chabinyc, *Adv. Mater.*, 2010, **22**, 3812–3838.

10 C. Y. Yang, W. L. Jin, J. Wang, Y. F. Ding, S. Y. Nong, K. Shi, Y. Lu, Y. Z. Dai, F. D. Zhuang, T. Lei, C. A. Di, D. Zhu, J. Y. Wang and J. Pei, *Adv. Mater.*, 2018, **30**, 9.

11 S. A. Gregory, A. K. Menon, S. Y. Ye, D. S. Seferos, J. R. Reynolds and S. K. Yee, *Adv. Energy Mater.*, 2018, **8**, 8.

12 H. Li, Z. Xu, J. Song, H. Y. Chai, L. L. Wu and L. D. Chen, *Adv. Funct. Mater.*, 2022, **32**, 9.

13 J. Liu, L. Qiu, R. Alessandri, X. K. Qiu, G. Portale, J. J. Dong, W. Talsma, G. Ye, A. A. Sengrian, P. C. T. Souza, M. A. Loi, R. C. Chiechi, S. J. Marrink, J. C. Hummelen and L. J. A. Koster, *Adv. Mater.*, 2018, **30**, 9.

14 F. Zhong, H. Li, Z. Xu, S. Y. Luo, J. Song and L. D. Chen, *ACS Appl. Polym. Mater.*, 2024, **6**, 15323–15331.

15 P. Durand, H. Y. Zeng, T. Biskup, V. Vijayakumar, V. Untilova, C. Kiefer, B. Heinrich, L. Herrmann, M. Brinkmann and N. Leclerc, *Adv. Energy Mater.*, 2022, **12**, 11.

16 E. H. Suh, J. G. Oh, J. Jung, S. H. Noh, T. S. Lee and J. Jang, *Adv. Energy Mater.*, 2020, **10**, 2002521.

17 D. Kiefer, R. Kroon, A. I. Hofmann, H. D. Sun, X. J. Liu, A. Giovannitti, D. Stegerer, A. Cano, J. Hynynen, L. Y. Yu, Y. D. Zhang, D. Q. Nai, T. F. Harrelson, M. Sommer, A. J. Moulé, M. Kemerink, S. R. Marder, I. McCulloch, M. Fahlman, S. Fabiano and C. Muller, *Nat. Mater.*, 2019, **18**, 149–155.

18 Z. M. Liang, Y. D. Zhang, M. Souri, X. Y. Luo, A. M. Boehm, R. P. Li, Y. Zhang, T. R. Wang, D. Y. Kim, J. G. Mei, S. R. Marder and K. R. Graham, *J. Mater. Chem. A*, 2018, **6**, 16495–16505.

19 S. E. Yoon, Y. Kang, G. G. Jeon, D. Jeon, S. Y. Lee, S. J. Ko, T. Kim, H. Seo, B. G. Kim and J. H. Kim, *Adv. Funct. Mater.*, 2020, **30**, 11.

20 H. Y. Chai, Z. Xu, H. Li, F. Zhong, S. Q. Bai and L. D. Chen, *ACS Appl. Electron. Mater.*, 2022, **4**, 4947–4954.

21 M. T. Fontana, D. A. Stanfield, D. T. Scholes, K. J. Winchell, S. H. Tolbert and B. J. Schwartz, *J. Phys. Chem. C*, 2019, **123**, 22711–22724.

22 D. A. Stanfield, Z. Mehmedovic and B. J. Schwartz, *Chem. Mat.*, 2021, **33**, 8489–8500.

23 I. E. Jacobs, E. W. Aasen, J. L. Oliveira, T. N. Fonseca, J. D. Roehling, J. Li, G. W. Zhang, M. P. Augustine, M. Mascal and A. J. Moulé, *J. Mater. Chem. C*, 2016, **4**, 3454–3466.

24 S. N. Patel, A. M. Glaudell, D. Kiefer and M. L. Chabinyc, *ACS Macro Lett.*, 2016, **5**, 268–272.

25 B. X. Dong, Z. W. Liu, M. Misra, J. Strzalka, J. Niklas, O. G. Poluektov, F. A. Escobedo, C. K. Ober, P. F. Nealey and S. N. Patel, *ACS Nano*, 2019, **13**, 7665–7675.

26 B. X. Dong, C. Nowak, J. W. Onorato, T. Z. Ma, J. Niklas, O. G. Poluektov, G. Grocke, M. F. DiTusa, F. A. Escobedo, C. K. Luscombe, P. F. Nealey and S. N. Patel, *Chem. Mat.*, 2021, **33**, 741–753.

27 K. Kang, S. Watanabe, K. Broch, A. Sepe, A. Brown, I. Nasrallah, M. Nikolka, Z. P. Fei, M. Heeney, D. Matsumoto, K. Marumoto, H. Tanaka, S. Kuroda and H. Sirringhaus, *Nat. Mater.*, 2016, **15**, 896–902.

28 R. J. Wen, H. H. Huang, J. Y. Wan, S. C. Wen, J. Z. Wang and X. Fan, *Energy Technol.*, 2021, **9**, 8.

29 T. Mukhopadhyaya, J. Wagner, T. D. Lee, C. Ganley, S. Tanwar, P. Raj, L. L. Li, Y. J. Song, S. J. Melvin, Y. Y. Ji, P. Clancy, I. Barman, S. Thon, R. S. Klausen and H. E. Katz, *Adv. Funct. Mater.*, 2024, **34**, 14.

30 J. Park, J. H. Song, J. G. Jang and J. Kwak, *Adv. Phys. Res*, 2024, 2400151.

31 R. Kroon, D. Kiefer, D. Stegerer, L. Y. Yu, M. Sommer and C. Müller, *Adv. Mater.*, 2017, **29**, 7.

32 M. Craighero, J. L. Guo, S. Zokaei, S. Griggs, J. F. Tian, J. Asatryan, J. Kimpel, R. Kroon, K. Xu, J. S. Reparaz, J. Martin, I. McCulloch, M. Campoy-Quiles and C. Müller, *ACS Appl. Electron. Mater.*, 2023, **6**, 2909–2916.

33 H. Li, J. Song, J. Xiao, L. L. Wu, H. E. Katz and L. D. Chen, *Adv. Funct. Mater.*, 2020, **30**, 10.

34 W. L. Liu, L. Müller, S. Y. Ma, S. Barlow, S. R. Marder, W. Kowalsky, A. Köhn and R. Lovrincic, *J. Phys. Chem. C*, 2018, **122**, 27983–27990.